Switchable-Hydrophilicity Triethylamine: Formation and Synergistic Effects of Asphaltenes in Stabilizing Emulsions Droplets

Xingang Li [1,2,3]**, Jinjian Hou** [1,2,]*****, Hong Sui** [1,2,3,]*****, Lingyu Sun** [1,2] **and Lin Xu** [1,2,4]

[1] School of Chemical Engineering and Technology, Tianjin University, Tianjin 300072, China; lxg@tju.edu.cn (X.L.); sunnixo@163.com (L.S.); 15822806749@163.com (L.X.)
[2] National Engineering Research Centre for Distillation Technology, Tianjin 300072, China
[3] Collaborative Innovation Center of Chemical Science and Engineering, Tianjin 300072, China
[4] China Academy of Safety Science and Technology, Beijing 100012, China
***** Correspondence: houjinjian@tju.edu.cn (J.H.); suihong@tju.edu.cn (H.S.); Tel.: +86-022-27404701 (J.H.)

check for updates

Abstract: In this study, SHT (switchable-hydrophilicity triethylamine, $[Et_3NH]\cdot[HCO_3]$) has been synthesized and instrumentally characterized by Fourier transform–infrared spectroscopy (FTIR) and ^{13}C nuclear magnetic resonance (NMR). The operational synthesis conditions of SHT were optimized and determined at 25 °C, Et_3N/H_2O volume ratio of 1:2 and CO_2 injection rate at 300 mL/min. When it was used to extract heavy oil from unconventional oil ore, it was found that it could break maltenes-in-water emulsions. When asphaltenes were present in the oil phase, it was observed that SHT could cooperate with asphaltenes. These results indicated that SHT works with asphaltenes, leading to synergistic effects in stabilizing oil–water (o/w) emulsions.

Keywords: switchable-hydrophilicity triethylamine (SHT); synergistic effect; emulsions stabilization; asphaltene

1. Introduction

Switchable hydrophilicity solvents (SHSs) are organic solvents with switchable miscibility between hydrophilicity and hydrophobicity [1,2]. Due to this property, SHS can be removed from the product and recycled without requiring distillation, potentially saving energy. Durelle et al. proposed a mathematical model to describe the behavior of CO_2-triggered switchable-hydrophilicity solvents in terms of their basicity and hydrophilicity [3]. The mathematical model facilitates the optimization of the synthesis of switchable-hydrophilicity solvent by adjusting pressure and the solvent/water volume ratio.

The application of these switchable hydrophilicity chemicals as process aids in oil extraction has been widely reported [4–12]. For instance, SHS could efficiently extract and recovery diesel from oil-based drill cuttings [8]. SHS could extract oil from Jatropha curcas L. oil seeds to produce biodiesel, and the extraction ratio is higher than hexane [10]. Some researchers found that SHS could extract phenols from lignin bio-oil, and 91% SHS could be recovered [12]. Besides, SHSs have been used in oil–sand separation as solvents or interfacial active materials [5–7,13]. During this oil–solid separation, the SHSs play important roles in modifying the oil–water (o/w) interface and oil–solid interface, resulting in the formation of oil–water emulsions [5]. The formation of emulsions during oil extraction makes the separation much more difficult [14,15]. However, little information has been reported on the exact mechanisms of SHS in stabilizing oil–water emulsions, especially its role together with natural interfacial active materials, such as asphaltenes [16–22].

In this paper, SHT will be formed and optimized. Its role in the stabilization of maltenes-in-water emulsions will be studied. Accordingly, the objectives of this study are to (i) find the optimal conditions for the formation of SHT; (ii) to understand the synergistic effect of SHT in stabilizing oil-water emulsions together with asphaltenes.

2. Experimental

2.1. Materials

Chemicals reagents, including toluene, n-heptane, Et_3N (triethylamine), hydrochloric acid, sodium hydroxide, and anhydrous sodium sulfate, were analytical grade purchased from Tianjin Jiangtian Technology Co. Ltd. (Tianjin, China). The Canadian oil sands samples were obtained from Athabasca, Canada. The composition of Athabasca oil sands was analyzed using the standard method to give 10.72 wt.% bitumen, 1.79 wt.% water, and 87.49 wt.% solids. The N_2 and CO_2 (of 99.9% purity) were purchased from Tianjin Liufang Technology Co. Ltd., China.

2.2. Optimization of Switchable-Hydrophilicity Triethylamine (SHT) Formation

Ten milliliters Et_3N and 10 mL deionized water were added into to a 100 mL three-neck round-bottom flask at 20 °C in a water bath. Then, a thermometer, 5 mm-diameter gas duct and exhaust pipe were placed in the flask. After the gas duct was inserted below the surface of the water, the CO_2 was injected into the liquid at a rate of 500 mL/min at atmospheric pressure. With the injection of CO_2 into the flask, the pH of the water phase decreased accordingly. The pH of the solution was measured using a pH meter in real time. Initially, there were two phases due to the immiscibility of the tertiary amines in water. Continued bubbling of CO_2 caused the phase interface to disappear, finally producing a homogeneous solution. The SHT concentration was highly dependent on the pH of the solution at a given temperature. When the pH remained stable, CO_2 injection was stopped. This meant that the homogenous solution was formed when the pH value change was within ±0.02. Then, the SHT solution was poured into a screw-neck glass bottle, and the anhydrous sodium sulfate was put into the SHT solution until the particles floated, which indicated that the water had been removed. The process was repeated by altering the temperature, triethylamine/water volume ratio and CO_2 injection rate according to a single factor experiment allowing the process parameters to be optimized.

2.3. Characterization

Fourier transform–infrared (FT–IR) spectra of SHT and Et_3N were measured using a FT–IR spectrometer (Bruker, Karlsruhe, Germany). For nuclear magnetic resonance (NMR) sample preparation, 200 µL Et_3N was dissolved in 800 µL of deuterated chloroform ($CDCl_3$ 99.8%-d) containing tetramethylsilane (TMS 0.3% v/v), and 200 µL SHT was dissolved in 800 µL D_2O. Subsequently, 600 µL of the mixture was transferred into a standard 5 mm NMR tube for direct measurement. The reagent was purchased from Aladdin (Shanghai, China). All one-dimensional ^{13}C-NMR spectra were recorded at 500 MHz and 298 K on a Bruker AV 600 spectrometer (Bruker Corporation, Faellanden, Switzerland) equipped with a cryoprobe and a z-gradient.

2.4. Emulsion Stability Experiment

The experimental procedures of the preparation of asphaltenes, maltenes, emulsions and demulsification are shown in Figure 1. The bitumen was extracted from 150 g oil sands through the toluene solvent extraction process. After extraction, the bitumen (2 g) was added to a conical flask, and 90 mL n-heptane was added. The bitumen was sonicated at 50 °C for 30 min. After sonication, the mixture was centrifuged at 8500 rpm for 15 min. After the centrifugation, the supernatant was transferred into a 500 mL conical flask. The insoluble solids were deposited back into the conical flask. The centrifugation and precipitation processes were repeated with additional 100 milliliters n-heptane

until the supernatant was colorless. The n-heptane was removed by a rotary evaporator, leaving the maltenes. Then, the insoluble solids were dried in a vacuum oven at 80 °C, and the solids were the asphaltene samples. The maltenes were transferred into a flask to mix with the toluene, obtaining a mixture with maltenes at a concentration of 1.2%. The organic phase was adjusted by adding SHT, asphaltenes or Et$_3$N. Twenty milliliters deionized water and 30 mL organic phase were mixed and transferred into a 100 mL round-bottom flask, and stirred at 900 rpm for 220 min. Then, the mixture was quickly transferred into a measuring cylinder, and the precipitated nonaqueous phase volume or aqueous phase volume were recorded.
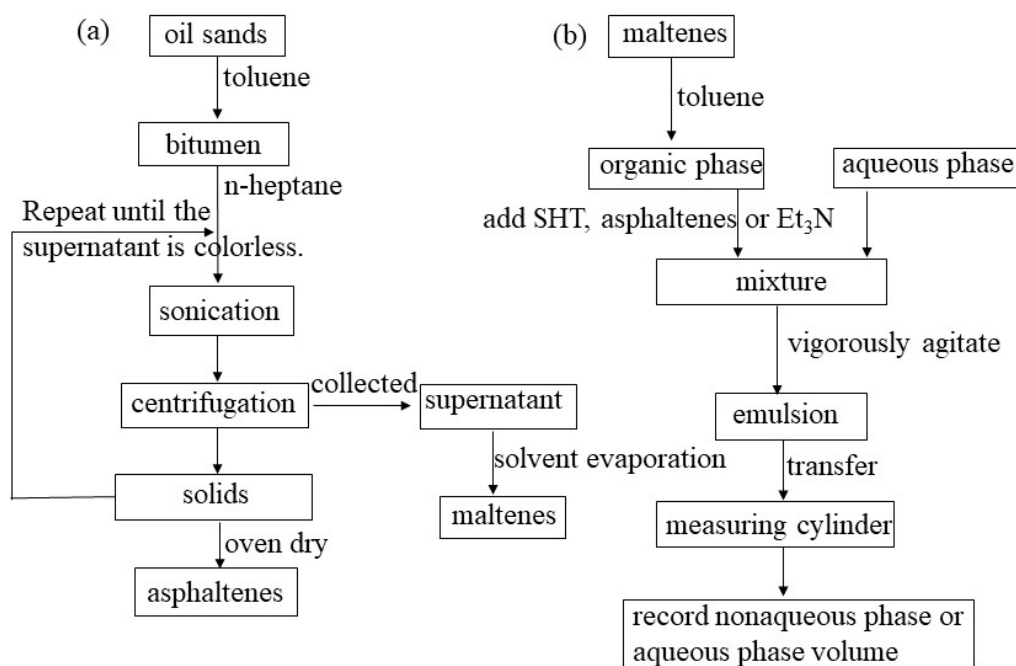
Figure 1. Schematic of the emulsion stability experiment procedures. (**a**) Preparation of asphaltenes and maltenes; (**b**) preparation of emulsions and the demulsification process.

2.5. Interfacial Tension (IFT) Measurements

The interfacial tension (IFT) between the non-aqueous phase and deionized water was measured by the pendant drop shape method (SL200B, Kino, Winslow, AZ, USA). The interfacial tension between the oil phase and water phase was measured based on the shape of a pendant drop using the asymmetric drop shape analysis technique, the similar experiment procedures could be found in the literature [6,23,24]. The temperature was 25 °C. The organic phase was injected into the water phase using a U-shape bent needle fixed on a micro-syringe. The experimental instrument could fit a theoretical Young–Laplace curve according to the drop shape. The drop got bigger when the organic phase injected by manual. The injection stopped until the drop shape was the biggest, and the drop would fall off if we continued increasing liquid when the drop shape was the biggest. Until the fitted curve was stable and unchanged, the fitted value was the IFT. The IFT of toluene/water is 36.1 mN/m, which indicated that the IFT measurement is accurate. Each measurement was repeated at least three times until the results were constant.

3. Results and Discussion

When Et$_3$N is exposed to CO$_2$, it is hydrophilic and even has complete miscibility in water. The CO$_2$ injection is stopped until the interface between the two immiscible phases disappears

(Figure 2b), which means that the reaction reached the equilibrium state and the SHT solution formed. The equation of SHT formation is [1,24]:

$$(CH_3CH_2)_3N + H_2O + CO_2 \rightleftarrows \left[(CH_3CH_2)_3NH\right]\left[HCO_3\right] \tag{1}$$
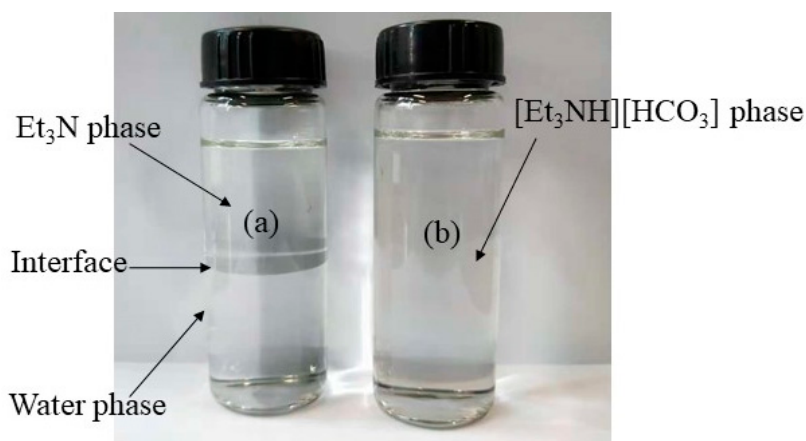
Figure 2. (**a**) The Et_3N oil phase and water phase coexist in the trimethylamine-water system with an interface between them; (**b**) one homogenous phase appears in the SHT solution after CO_2 addition.

3.1. Characterizations of SHT

3.1.1. Fourier Transform–Infrared (FT–IR) Analysis

To further detect whether SHT has been synthesized successfully, Et_3N and SHT were characterized by FT–IR, as shown in Figure 3. Obviously, the characteristic bands for Et_3N were mainly located at 3000–2800 cm^{-1} (the stretching vibration of saturated C–H bonds) and 1385–1060 cm^{-1} (the stretching vibration of C–N bonds). The characteristic bands for SHT were mainly located at 3500–3400 cm^{-1}, 3000–2800 cm^{-1}, 1700–1600 cm^{-1} and 1500–1000 cm^{-1}. The strong and broad band at 3445 cm^{-1} was associated with the –N–H stretching vibration in $[(CH_3CH_2)_3NH]^+$. The bands at about 2974 cm^{-1} and 2941 cm^{-1} represented the C–H asymmetrical stretching vibration of –CH$_3$, –CH$_2$–, respectively. In addition, the band at 1631 cm^{-1} was due to asymmetric C=O stretching vibration, which was from the $[HCO_3]^-$. The weak bands at about 1475 cm^{-1} and 1397 cm^{-1} represented the C–H scissoring vibration of –CH$_2$–, and asymmetrical deformation vibration of –CH$_3$, respectively. The other bands in the 1500–1000cm^{-1} range were due to the –C–N stretching vibration.
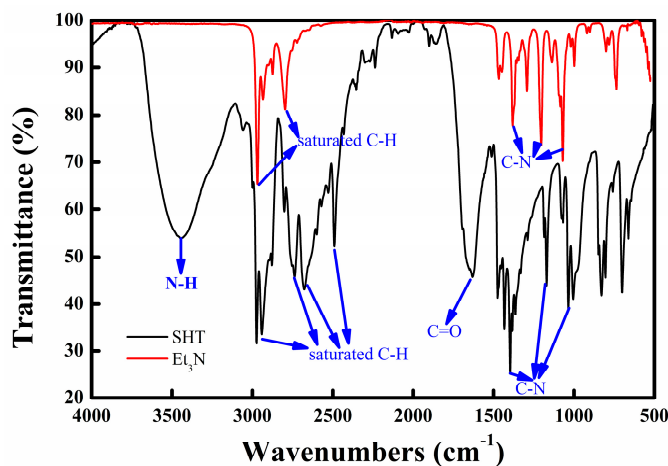
Figure 3. The Fourier transform–infrared (FT–IR) spectra of Et_3N and SHT.

3.1.2. ^{13}C Nuclear Magnetic Resonance (NMR) Analysis

Et$_3$N and SHT were characterized by ^{13}C-NMR spectra, as shown in Figure 4. The chemical shifts of Et$_3$N at 11.78 and 46.40 ppm were assigned to the –CH$_3$ and –CH$_2$– groups, the solvent peak is found at 77.33 ppm (Figure 4a). The chemical shifts of SHT at 8.13 and 46.47 ppm were assigned, respectively, to the –CH$_3$ and –CH$_2$– groups of [(CH$_3$CH$_2$)$_3$NH]$^+$ while that at 160.15 ppm was attributed to the carbon atom of [HCO$_3$]$^-$ (Figure 4b). These indicated that SHT has formed successfully.
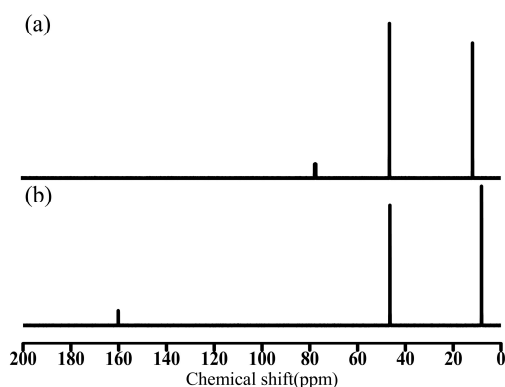
**Figure 4.** The ^{13}C nuclear magnetic resonance (NMR) spectra of (**a**) Et$_3$N in CDCl$_3$, (**b**) SHT in D$_2$O.

3.2. Optimization of the Formation Process

Equation (2) describes the percentage (P) of protonated tertiary amines [3]. The protonation is dependent on solution pH and the acid dissociation constant (K$_{aH}$) of Et$_3$N. It is only related to the [H]$^+$ concentration at the specific temperature for Et$_3$N; therefore, pH is the indicator of reaction equilibrium.

$$P = \frac{[H]^+}{[H]^+ + K_{aH}} \times 100\%$$

(2)

The temperature and the concentration of reactants influence the chemical equilibrium and reaction rate. The temperature, amine/water volume ratio and CO$_2$ injection rate are optimized (Figure 5). When the temperature increases from 15 °C to 35 °C, the reaction rate increases sharply, then pH decreasing slope is increasing with the temperature increase, so when the reaction did not reach equilibrium, the pH (35 °C) is lower than the pH (15 °C) when the reaction time is less than 45 min. Because the reaction is exothermic, when the temperature increases the conversion decreases, therefore the equilibrium pH of the solution increases. When the reaction reaches equilibrium, the pH was shown that black line (15 °C) < red line (25 °C) < blue lines (35 °C). The optimal temperature is determined to be 25 °C. With increasing Et$_3$N/water volume ratio, the reaction rate sharply increases, allowing the ultimate pH to be decreased. This suggests that the conversion increases. However, when the Et$_3$N/water volume ratio is less than 1:2, the pH changes little. Therefore, the optimal Et$_3$N/water volume ratio is 1:2. The reaction rate also increases with the increase of the CO$_2$ injection rate, but CO$_2$ conversion decreases. When 10 mL Et$_3$N is used and the reaction equilibrium is reached, 1.6 L CO$_2$ is in theory needed. The equilibrium time for 100 mL/min was 110 min, but for 300 mL/min it was 55 min. The total CO$_2$ supply at equilibrium time for 100 mL/min and 300 mL/min was 11 L and 16.5 L, respectively; the CO$_2$ availability was 15% and 10%, respectively. The reaction rate accelerates with the higher CO$_2$ injecting rate, and then the equilibrium time decreases. The CO$_2$ availability decreases when the CO$_2$ injection rate increases. When the CO$_2$ is 500 mL/min, the line (was not shown in Figure 5) was similar to the red line (300 mL/min), so increasing CO$_2$ injection rate to 500 mL/min was meaningless. The optimal conditions are as follows: temperature of 25 °C; tertiary amine to water volume ratio of 1:2; CO$_2$ gas injecting rate of 300 mL/min.
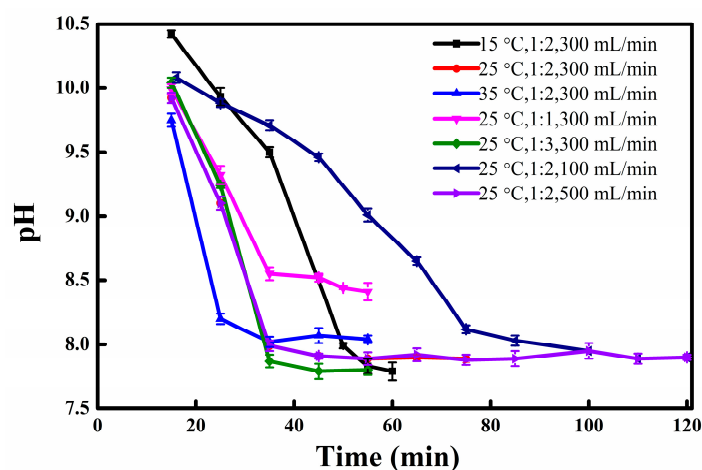
Figure 5. The variation of solution pH as a function of reaction time at different temperatures, Et_3N/H_2O volume ratios, and CO_2 injecting rates.

3.3. The Role of SHT in Emulsion Stabilization

The role of asphaltenes in stabilizing maltenes-in-water emulsions can also be ascertained by comparing the emulsions with different asphaltene contents, as shown in Figures 6 and 7–c. It can be seen that the emulsions made by the organic phase containing asphaltenes are much more stable. The ate of demulsification becomes slower and the amount of emulsions increases when the asphaltene content in the oil phase increases. Asphaltenes formed a rigid skin at the oil–water interface, allowing the stability of the emulsions to be improved [25,26].

The role of Et_3N or SHT in stabilizing maltenes-in-water emulsions is shown in Figures 6a and 7d,e. Since the demulsification of maltene–water emulsions by SHT is too fast to observe, the water phase is used to quantify the volume of emulsions. Comparing Figure 7d,e, SHT could accelerate demulsification but Et_3N could stabilize emulsions. After SHT dissolves into the aqueous phase, the anion and cation compress the double electric layer. As a result, the zeta potential decreases, leading to a reduction in the interaction force. It is easy for these oil droplets to collide and coalesce under van der Waals force and, therefore, the emulsions are broken. Comparing Figure 7a,e, SHT shows the demulsification effect, and the theory is similar to electrolyte demulsification. Although SHT could individually accelerate the demulsification process, the synergistic effect of SHT and asphaltenes on stabilizing maltenes-in-water emulsions is obvious (as shown in Figure 6a).
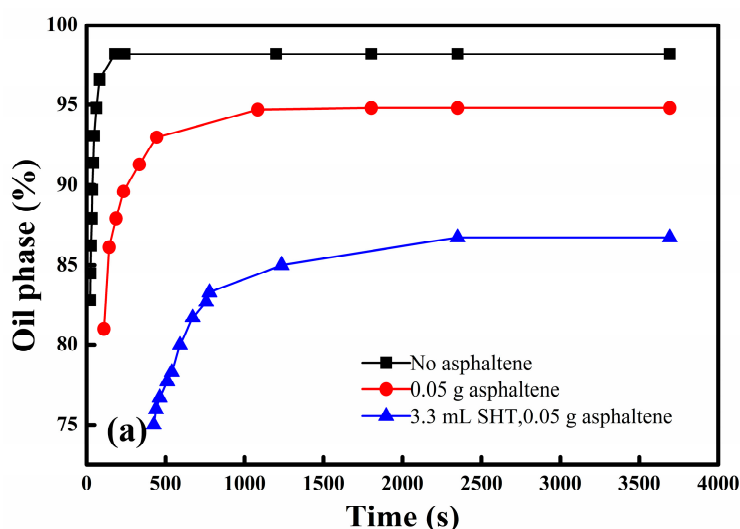
Figure 6. *Cont.*
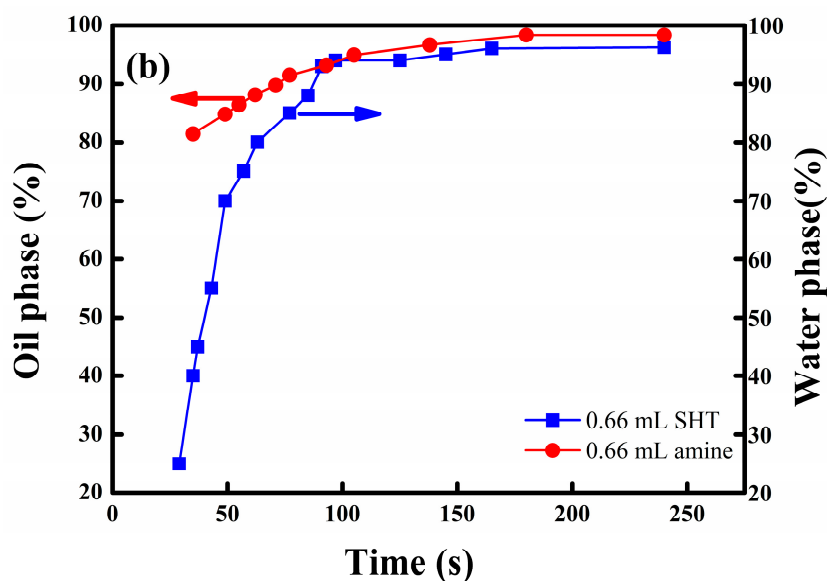
Figure 6. The effect of (**a**) asphaltene (1.7 g/L) and SHT content SHT (11%); (**b**) SHT (2.2%) (without asphaltenes) and Et3N (2.2 %) (without asphaltenes) on the stability of maltenes-in-water emulsions.
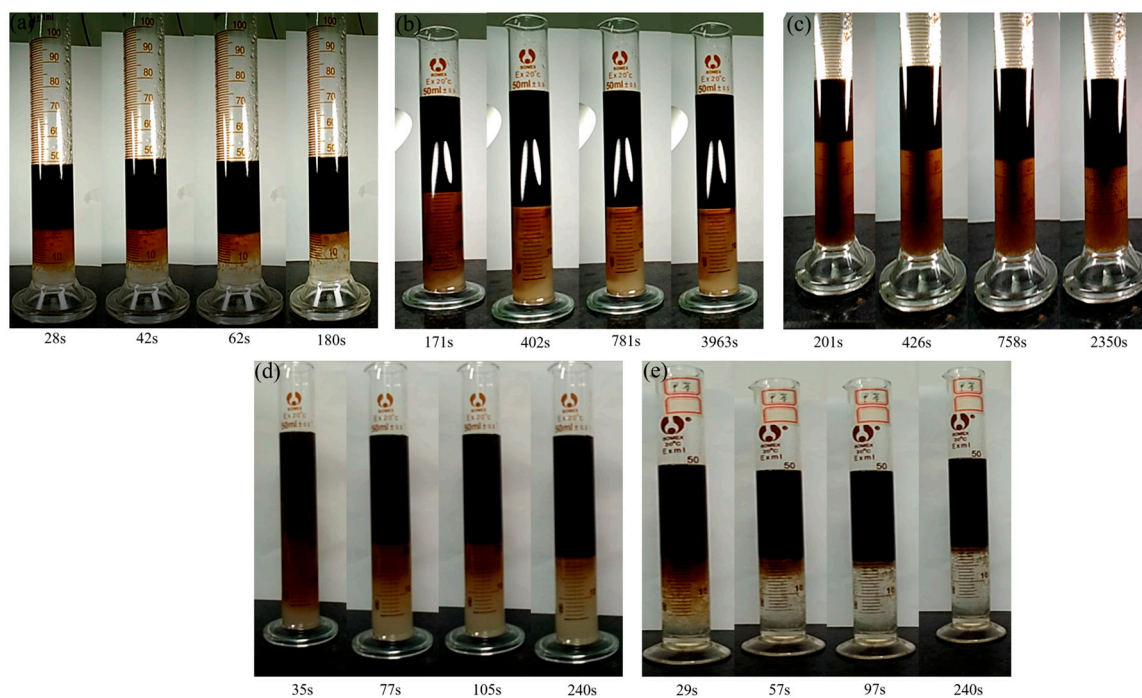

Figure 7. Visual appearance of emulsions at room temperature (**a**) without asphaltenes, SHT, and Et$_3$N; (**b**) asphaltenes (1.7 g/L); (**c**) SHT (11%) and asphaltenes (1.7 g/L); (**d**) Et3N (2.2%); (**e**) SHT (2.2%).

3.4. IFT of the Oil and Water

As shown in Figure 8, the interfacial tension decreases from 33.7 mN/m to 7.4 mN/m, when the asphaltene content increases from 0 to 17 g/L. Asphaltenes can adsorb at the oil-water interface; they form a protective layer; the oil-water interfacial tension decreases, and the layer could stabilize emulsions [25,27]. The interfacial tension decreases from 33.7 mN/m to 13.2 mN/m, when the SHT content increases from 0 to 11%. SHT works as a surfactant because it can decrease the oil–water interfacial tension, and this phenomenon can be found in the literature [6]. SHT enhances the adsorption of asphaltenes at the o/w interface, because the interfacial tension decreases from

23.9 mN/m to 21.6 mN/m when SHT is added to the asphaltene solution. Et_3N could decrease the o/w interfacial tension from 33.7 mN/m to 23.6 mN/m. SHT easily resolves Et_3N under N_2, and both SHT and Et_3N can decrease the oil–water interfacial tension. The combination of asphaltenes and SHT is observed to be helpful for the reduction of the oil–water interfacial tension.
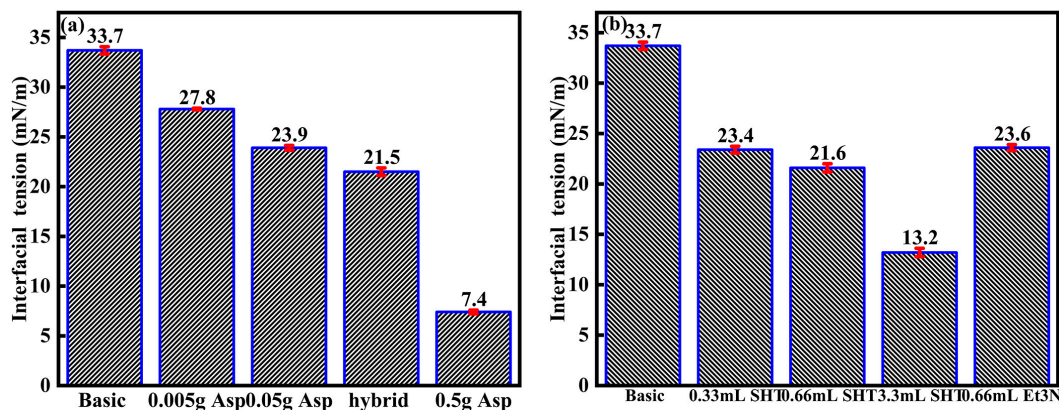
Figure 8. The oil–water interfacial tension as a function of asphaltenes content, SHT content, and Et_3N content at ambient conditions ("hybrid" means 0.33 mL SHT and 0.05 g asphaltenes).

3.5. The Mechanism of SHT and Asphaltenes' Synergistic Effect on Stabilizing the Emulsions

The synergistic effect of SHT and asphaltenes on stabilizing maltenes-in-water emulsions is shown in Figure 9. SHT can help asphaltenes to adsorb at the o/w interface by forming ion pairs. It is easy to transfer the oil–water interface and this helps asphaltenes adsorb at the o/w interface. Asphaltenes that accumulate at the oil-water interface could hinder demulsification. Asphaltenes could adsorb at the oil–water interface by themselves, and the presence of SHT will facilitate the stability of the oil–water emulsions.
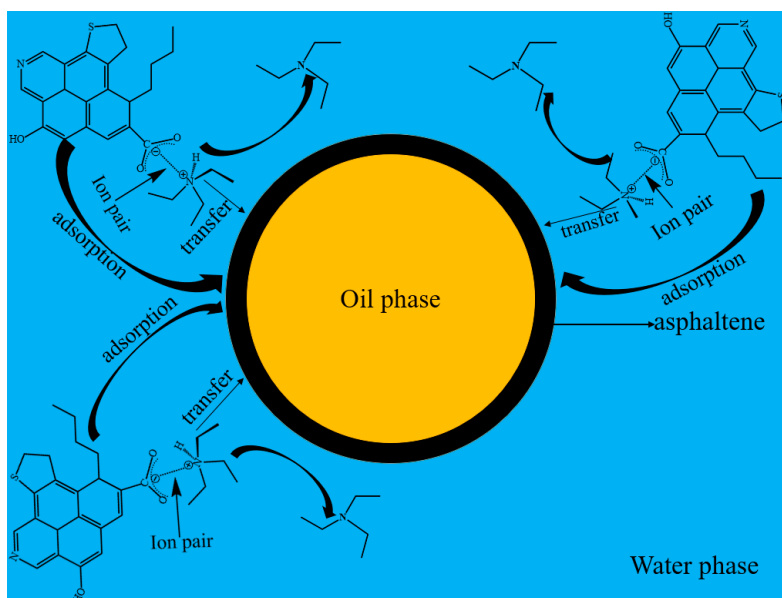
Figure 9. The mechanism of the synergistic effect between SHT and asphaltenes in stabilizing the emulsions.

4. Conclusions

The formation conditions for SHT have been optimized by operational tests. The optimal conditions are determined at 25 °C with the triethylamine to water volume ratio of 1:2, and the

CO_2 injecting rate at 300 mL/min. It is found that SHT and Et_3N can work as a surfactant to decrease the oil–water interfacial tension. However, only Et_3N can stabilize the emulsions, while SHT can help to break the maltene–water emulsions. When asphaltenes are present in the oil, SHT is found to be able to work together with asphaltenes to stabilize maltenes-in-water emulsions. The improvement in the stability of emulsions by SHT and asphaltenes can be mainly attributed to the interaction between SHT and asphaltenes by forming $[Et_3NH]^+$-asphaltene ion pairs at the oil–water interface.

Author Contributions: Conceptualization, X.L., J.H. and H.S.; Formal analysis, X.L., J.H., H.S. and L.S.; Investigation, X.L., J.H. and L.X.; Resources, X.L.; Writing—original draft, X.L. and J.H.; Writing—review and editing, H.S., L.S. and L.X.

Conflicts of Interest: The authors declare no conflict of interests.

References

1. Jessop, P.G.; Kozycz, L.; Rahami, Z.G.; Schoenmakers, D.; Boyd, A.R.; Wechsler, D.; Holland, A.M. Tertiary amine solvents having switchable hydrophilicity. *Green Chem.* **2011**, *13*, 619–623. [CrossRef]
2. Pollet, P.; Eckert, C.A.; Liotta, C.L. Switchable solvents. *Chem. Sci.* **2011**, *2*, 609–614. [CrossRef]
3. Durelle, J.; Vanderveen, J.R.; Jessop, P.G. Modelling the behavior of switchable-hydrophilicity solvents. *Phys. Chem. Chem. Phys.* **2014**, *16*, 5270–5275. [CrossRef] [PubMed]
4. Phan, L.; Brown, H.; White, J.; Hodgson, A.; Jessop, P.G. Soybean oil extraction and separation using switchable or expanded solvents. *Green Chem.* **2009**, *11*, 53–59. [CrossRef]
5. Sui, H.; Xu, L.; Li, X.; He, L. Understanding the roles of switchable-hydrophilicity tertiary amines in recovering heavy hydrocarbons from oil sands. *Chem. Eng. J.* **2016**, *290*, 312–318. [CrossRef]
6. Li, X.; Yang, Z.; Sui, H.; Jain, A.; He, L. A hybrid process for oil-solid separation by a novel multifunctional switchable solvent. *Fuel* **2018**, *221*, 303–310. [CrossRef]
7. Holland, A.; Wechsler, D.; Patel, A.; Molloy, B.M.; Boyd, A.R.; Jessop, P.G. Separation of Bitumen from Oil Sands using a Switchable Hydrophilicity Solvent. *Can. J. Chem.* **2012**, *90*, 805–810. [CrossRef]
8. Wang, S.; Zheng, C.; Zhao, J.; Li, X.; Lu, H. Extracting and recovering diesel from oil-based drill cuttings using switchable hydrophilic solvents. *Chem. Eng. Res. Des.* **2017**, *128*, 27–36. [CrossRef]
9. Samori, C.; Cespi, D.; Blair, P.; Galletti, P.; Malferrari, D.; Passarini, F.; Vassura, I.; Tagliavini, E. Application of switchable hydrophilicity solvents for recycling multilayer packaging materials. *Green Chem.* **2017**, *19*, 1714–1720. [CrossRef]
10. Zeng, S.; Tao, C.; Parnas, R.; Jiang, W.; Liang, B.; Liu, Y.; Lu, H. *Jatropha curcas* L. oil extracted by switchable solvent *N*, *N*-dimethylcyclohexylamine for biodiesel production. *Chin. J. Chem. Eng.* **2016**, *24*, 1640–1646. [CrossRef]
11. Du, Y.; Schuur, B.; Kersten, S.R.A.; Brilman, D.W.F. Opportunities for switchable solvents for lipid extraction from wet algal biomass: An energy evaluation. *Algal Res.* **2015**, *11*, 271–283. [CrossRef]
12. Fu, D.; Farag, S.; Chaouki, J.; Jessop, P.G. Extraction of phenols from lignin microwave-pyrolysis oil using a switchable hydrophilicity solvent. *Bioresour. Technol.* **2014**, *154*, 101–108. [CrossRef] [PubMed]
13. Lin, F.; Stoyanov, S.R.; Xu, Y. Recent Advances in Nonaqueous Extraction of Bitumen from Mineable Oil Sands: A Review. Org. *Process Res. Dev.* **2017**, *21*, 492–510. [CrossRef]
14. Pensini, E.; Harbottle, D.; Yang, F.; Tchoukov, P.; Li, Z.; Kailey, I.; Behles, J.; Masliyah, J.; Xu, Z. Demulsification mechanism of asphaltene-stabilized water-in-oil emulsions by a polymeric ethylene oxide–propylene oxide demulsifier. *Energy Fuels* **2014**, *28*, 6760–6771. [CrossRef]
15. Kupai, M.M.; Yang, F.; Harbottle, D.; Moran, K.; Masliyah, J.; Xu, Z. Characterising rag-forming solids. *Can. J. Chem. Eng.* **2013**, *91*, 1395–1401. [CrossRef]
16. Zhang, J.; Tian, D.; Lin, M.; Yang, Z.; Dong, Z. Effect of Resins, Waxes and Asphaltenes on Water-Oil Interfacial Properties and Emulsion Stability. *Colloids Surf. A Physicochem. Eng. Asp.* **2016**, *507*, 1–6. [CrossRef]

17. Yarranton, H.W.; Hussein, H.; Masliyah, J.H. Water-in-Hydrocarbon Emulsions Stabilized by Asphaltenes at Low Concentrations. *J. Colloid Interface Sci.* **2000**, *228*, 52–63. [CrossRef] [PubMed]

18. Yang, F.; Tchoukov, P.; Dettman, H.D.; Teklebrhan, R.B.; Liu, L.; Dabros, T.; Czarnecki, J.; Xu, Z. Asphaltene sub-fractions responsible for stabilizing water-in-crude oil emulsions: Part 2. Molecular representations and molecular dynamic simulations. *Energy Fuels* **2015**, *31*, 9179–9187.

19. Yang, F.; Tchoukov, P.; Pensini, E.; Dabros, T.; Czarnecki, J.; Masliyah, J.; Xu, Z. Asphaltene Subfractions Responsible for Stabilizing Water-in-Crude Oil Emulsions. Part 1: Interfacial Behaviors. *Energy Fuels* **2014**, *28*, 6897–6904. [CrossRef]

20. Shi, C.; Zhang, L.; Xie, L.; Lu, X.; Liu, Q.; Mantilla, C.A.; Fg, V.D.B.; Zeng, H. Interaction Mechanism of Oil-in-Water Emulsions with Asphaltenes Determined Using Droplet Probe AFM. *Langmuir* **2016**, *32*, 2302–2310. [CrossRef] [PubMed]

21. Qiao, P.; Harbottle, D.; Tchoukov, P.; Wang, X.; Xu, Z. Asphaltene Subfractions Responsible for Stabilizing Water-in-Crude Oil Emulsions. Part 3: Effect of Solvent Aromaticity. *Energy Fuels* **2017**, *31*, 9179–9187. [CrossRef]

22. Mcgurn, M.K.; Baydak, E.N.; Sztukowski, D.M.; Yarranton, H.W. The Effect of Inorganic Solids on Emulsion Layer Growth in Asphaltene-Stabilized Water-in-Oil Emulsions. *Can. J. Chem. Eng.* **2017**, *95*, 1909–1924. [CrossRef]

23. Zolghadr, A.; Escrochi, M.; Ayatollahi, S. Temperature and Composition Effect on CO_2 Miscibility by Interfacial Tension Measurement. *J. Chem. Eng. Data* **2013**, *58*, 1168–1175. [CrossRef]

24. Jessop, P.G.; Phan, L.; Carrier, A.; Robinson, S.; Dürr, C.J.; Harjani, J.R. A solvent having switchable hydrophilicity. *Green Chem.* **2010**, *12*, 809–814. [CrossRef]

25. Liu, J.; Zhao, Y.; Ren, S. Molecular Dynamics Simulation of Self-Aggregation of Asphaltenes at an Oil/Water Interface: Formation and Destruction of the Asphaltene Protective Film. *Energy Fuels* **2015**, *29*, 1233–1242. [CrossRef]

26. Teklebrhan, R.B.; Ge, L.; Bhattacharjee, S.; Xu, Z.; Sjöblom, J. Initial partition and aggregation of uncharged polyaromatic molecules at the oil-water interface: A molecular dynamics simulation study. *J. Phys. Chem. B* **2014**, *118*, 1040–1051. [CrossRef] [PubMed]

27. Zhang, S.; Zhang, L.; Lu, X.; Shi, C.; Tang, T.; Wang, X.; Huang, Q.; Zeng, H. Adsorption kinetics of asphaltenes at oil/water interface: Effects of concentration and temperature. *Fuel* **2018**, *212*, 387–394. [CrossRef]